UCLA
COMPUTATIONAL AND APPLIED MATHEMATICS

Active Contours Without Edges

Tony F. Chan
Luminita Vese

December 1998

CAM Report 98-53

Department of Mathematics
University of California, Los Angeles
Los Angeles, CA. 90095-1555

http://www.math.ucla.edu/applied/cam/index.html

Active contours without edges

Tony F. Chan and Luminita A. Vese

Abstract— **In this paper, we propose a new model for active contours to detect objects in a given image, based on techniques of curve evolution, Mumford-Shah functional for segmentation and level sets. Our model can detect objects whose boundaries are not necessarily defined by gradient. We minimize an energy which can be seen as a particular case of the so-called minimal partition problem. In the level set formulation, the problem becomes a "mean-curvature flow"-like evolving the active contour, which will stop on the desired boundary. However, the stopping term does not depend on the gradient of the image, as in the classical active contour models, but is instead related to a particular segmentation of the image. We will show existence of minimizers for our problem and propose an algorithm using level sets and finite differences. Finally, we will present various experimental results and in particular some examples for which the classical snakes methods based on the gradient are not applicable. We will also see that interior contours are automatically detected and that the initial curve can start anywhere in the image, and not only around or inside the desired objects.**

Keywords— **Snakes, active contours, energy minimization, partial differential equations, segmentation, level sets, functions of bounded variation, finite differences.**

I. Introduction

The basic idea in active contour models or snakes is to evolve a curve, subject to constraints from a given image u_0, in order to detect objects in that image. For instance, starting with a curve around the object to be detected, the curve moves toward its interior normal and has to stop on the boundary of the object.

We first recall some of the classical active contour models or snakes ([13], [5], [16], [6]). Let Ω be a bounded and open subset of $I\!R^N$, with $\partial\Omega$ its boundary. Let u_0 be a given image, as a bounded function defined on $\overline{\Omega}$ and with real values. For $N = 2$, $\overline{\Omega}$ is a rectangle in the plane and u_0 takes values between 0 and 255. Denote by $C(s) : [0,1] \to I\!R^2$ a piecewise $C^1[0,1]$ parameterized curve.

In all the classical snakes and active contour models, an edge detector is used to stop the evolving curve on the boundaries of the desired object. Usually, this is a positive, decreasing and regular edge-function $g(|\nabla u_0|)$, such that $\lim_{t\to\infty} g(t) = 0$. For instance,

$$g(|\nabla u_0|) = \frac{1}{1 + |\nabla G_\sigma * u_0|^p}, \; p \geq 1,$$

where $G_\sigma * u_0$, a smoother version of u_0, is the convolution of the image u_0 with the Gaussian $G_\sigma(x,y) = \sigma^{-1/2} e^{-|x^2+y^2|/4\sigma}$. The function $g(|\nabla u_0|)$ is strictly positive in homogeneous regions, and near zero on the edges.

The snake model [13] is: $\inf_C J_1(C)$, where

$$J_1(C) = \int_0^1 |C'(s)|^2 ds + \lambda \int_0^1 g(|\nabla u_0(C(s))|)^2 ds. \quad (1)$$

The first term in (1) is the internal energy and controls the smoothness of the curve (we considered here only the rigidity term, with the first order derivative; the elasticity term, with the second order derivative can also be added). The second term is the external energy and attracts the contour towards the edges of the object in the image u_0.

In problems of curve evolution, the level set method and in particular the mean curvature motion of S. Osher and J. Sethian [20] have been used extensively, because it allows for cusps, corners, and automatic topological changes. Moreover, the discretization of the problem is made on a fixed regular grid.

We now recall the equation which governs the motion by mean curvature [20] in any dimension N:

$$\begin{cases} \frac{\partial \phi}{\partial t} = |\nabla \phi| \mathrm{div}\left(\frac{\nabla \phi}{|\nabla \phi|}\right), \\ \phi(0,x) = \phi_0(x), \; t \in [0,\infty), \; x \in I\!R^N. \end{cases}$$

Here, $\phi(t,\cdot)$ is the level set function, assumed to be Lipschitz. By this evolution equation, the level sets of ϕ, $\{x \in I\!R^N : \phi(t,x) = c\}$ move in the normal direction with a speed equal to the mean curvature. Once we start with an initial curve, which is the zero

This work was supported in part by ONR Contract N00014-96-1-0277 and NSF Contract DMS-9626755.

Address: UCLA, Mathematics Department, 405 Hilgard Avenue, Los Angeles, California 90095-1555.

e-mails: chan, lvese @math.ucla.edu.

Internet address: http://www.math.ucla.edu/applied/.

level set of ϕ_0 and such that ϕ_0 has opposite signs inside and outside the curve, we can follow the zero level curve of $\phi(t)$ and this gives a representation for evolving curves by mean curvature. The operator $K(\phi)(x) = \text{div}\left(\frac{\nabla\phi(x)}{|\nabla\phi(x)|}\right)$ represents the curvature of the level-curve of ϕ passing through x.

A geometric active contour model based on the mean curvature motion is given by the following evolution equation [5]:

$$\begin{cases} \frac{\partial\phi}{\partial t} = g(|\nabla u_0|)|\nabla\phi|\left(\text{div}\left(\frac{\nabla\phi}{|\nabla\phi|}\right) + \nu\right), \\ \text{in } [0,\infty[\times I\!R^2 \\ \phi(0,x) = \phi_0(x) \text{ in } I\!R^2, \end{cases} \tag{2}$$

where $g(|\nabla u_0|)$ is the edge-function defined before with $p = 2$, and ν is a positive constant. ϕ_0 is the initial level set function. Its zero level curve moves in the normal direction with the velocity $g(|\nabla u_0|)(K(\phi)(x)+\mu)$ and therefore stops on the desired boundary, where g vanishes. The constant ν is a correction term chosen so that $\text{div}\left(\frac{\nabla\phi(x)}{|\nabla\phi(x)|}\right)+\nu$ remains always positive. This constant may be interpreted as a force pushing the curve toward the object, when the curvature becomes null or negative (on the other hand, the presence of the constant ν is a constraint on the area inside the curve, and this also increases the propagation speed).

Other active contour models based on level sets were proposed in [16], again based on the image gradient. The first is

$$\begin{cases} \phi_t = |\nabla\phi|(-\nu + \frac{\nu}{(M_1-M_2)}(|\nabla G_\sigma * u_0(x)| - M_2)), \\ \phi(0,x) = \phi_0(x) \text{ in } I\!R^2, \end{cases}$$

where ν is a constant, and M_1 and M_2 are the maximum and minimum values of the magnitude of image gradient $|\nabla G_\sigma * u_0(x)|$. The second model [16] is similar to the geometric model [5], but with $p = 1$. Related works can be found for instance in [17] and [18].

The geodesic model [6] is:

$$\inf_C J_2(C) = 2\int_0^1 |C'(s)| \cdot g(|\nabla u_0(C(s)|)ds. \tag{3}$$

This is a problem of geodesic computation in a Riemannian space, according to a metric induced by the image u_0. Solving the minimization problem (3) consists in finding the path of minimal new length in that metric.

The equivalence between the models (1) and (3) is proved in two different ways in [6] and [1].

The geodesic active contour model [6] has also a level set formulation:

$$\begin{cases} \frac{\partial\phi}{\partial t} = |\nabla\phi|(\text{div}(g(|\nabla u_0|)\frac{\nabla\phi}{|\nabla\phi|}) + \nu g(|\nabla u_0|)), \\ \text{in } [0,\infty[\times I\!R^2 \\ \phi(0,x) = \phi_0(x) \text{ in } I\!R^2. \end{cases} \tag{4}$$

Here again the constant ν is added to increase the evolution speed and to attracts the curve towards the boundary and constitutes in fact an extra area-based speed.

Because all these classical snakes or active contour models rely on the edge-function g, depending on the image gradient $|\nabla u_0|$, to stop the curve evolution, these models can detect only objects with edges defined by gradient. Also, in practice, the discrete gradients are bounded and then the stopping function g is never zero on the edges, and the curve may pass through the boundary. On the other hand, if the image u_0 is very noisy, then the isotropic smoothing Gaussian has to be strong, which will smooth the edges too. In this paper, we propose a different active contour model, without a stopping edge-function, i.e. a model which is not based on the gradient of the image u_0 for the stopping process. The stopping term is based on Mumford-Shah segmentation techniques [19]. In this way, we obtain a model which can detect contours both with or without gradient, for instance objects with very smooth boundaries or even with discontinuous boundaries (for a discussion on different types of contours, we refer the reader to [12]). Moreover, our model has a level set formulation. Also, interior contours are automatically detected and the initial curve can start anywhere in the image.

The outline of the paper is as follows. In the next section we introduce our model as an energy minimization and discuss the relationship with the Mumford-Shah functional for segmentation. Also, we formulate the model in terms of level set functions, study the existence of minimizers and compute the associated Euler-Lagrange equations. In Section 3 we present an iterative algorithm for solving the problem and its discretization. Finally, we validate our model by various numerical results on synthetic and real images, showing the advantages of our model described before, and we end the paper by a brief concluding section.

Before describing our model, we would like to refer the reader to the following related works: [27] and [25] on active contours, [29] and [14] on shape reconstruction from unorganized points, and finally to recent works [21] and [22], where a probability based

geodesic active region model combined with classical gradient based active contour techniques is proposed.

II. Description of the Model

Our model is the minimization of an energy based-segmentation. Let us first explain the basic idea of the model in a simple case. Assume that the image u_0 is formed by two regions of approximatively piecewise-constant intensities, of distinct values u_0^i and u_0^o and that the object to be detected is represented by the region with the value u_0^i. Let denote its boundary by C_0. Then we have $u_0 \approx u_0^i$ inside the object (or inside C_0) and $u_0 \approx u_0^o$ outside the object (or outside C_0). Now let us consider the following "fitting energy":

$$\begin{aligned} & F_1(C) \quad + \quad F_2(C) \\ = & \int_{inside(C)} |u_0 - c_1|^2 dx \quad + \quad \int_{outside(C)} |u_0 - c_2|^2 dx, \end{aligned}$$

where C is any other variable curve, and the constants c_1, c_2, depending on C, are the averages of u_0 inside C and respectively outside C. In this simple case, it is obvious that C_0, the boundary of the object, is the minimizer of the "fitting energy":

$$\inf_C \Big\{ F_1(C) + F_2(C) \Big\} \approx 0 \approx F_1(C_0) + F_2(C_0).$$

This can be seen easily. For instance, if the curve C is outside the object, then $F_1(C) > 0$ and $F_2(C) \approx 0$. If the curve C is inside the object, then $F_1(C) \approx 0$ but $F_2(C) > 0$. If the curve C is both inside and outside the object, then $F_1(C) > 0$ and $F_2(C) > 0$. Finally, the fitting energy is minimized if $C = C_0$, i.e. if the curve C is on the boundary of the object. These basic remarks are illustrated in Fig. 1.

In our active contour model we will minimize this fitting energy and we will add some regularizing terms, like the length of C and/or the area inside C. Therefore, we introduce the energy $F(C, c_1, c_2)$ defined by:

$$F(C, c_1, c_2) = \mu \cdot (\text{length}(C))^p + \nu \cdot \text{area}(inside C)$$

$$+\lambda_1 \int_{inside(C)} |u_0 - c_1|^2 dx + \lambda_2 \int_{outside(C)} |u_0 - c_2|^2 dx,$$

where c_1 and c_2 are constant unknowns, and $\mu \geq 0$, $\nu \geq 0$, $\lambda_1, \lambda_2 > 0$ are fixed parameters. Of-course that one of these parameters can be "eliminated", by fixing it to be 1. In almost all our numerical calculations, we fix $\lambda_1 = \lambda_2 = 1$, and $\nu = 0$, i.e. we do not need the area term in the energy (this term can be used when for instance we may need to force the curve to move only inside, or only outside).

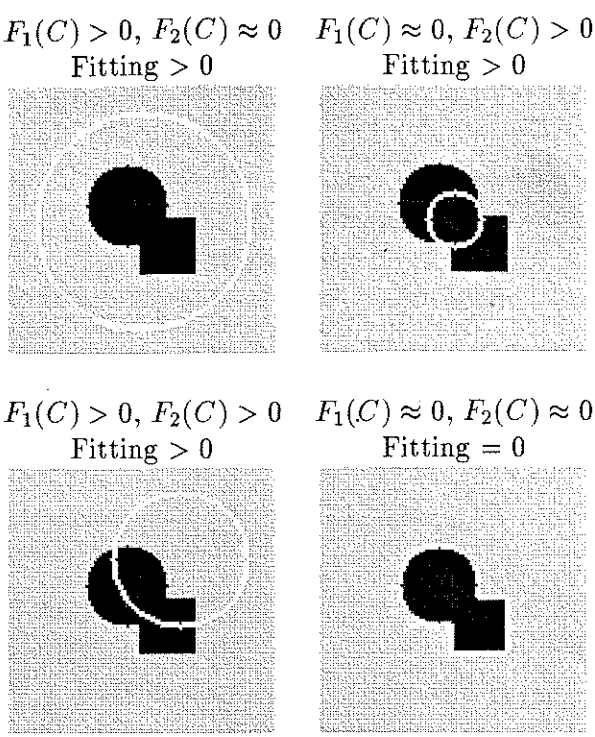

Fig. 1. Consider all possible cases in the position of the curve. The "fitting energy" is minimized only for the case when the curve is on the boundary of the object.

In general, we can take $p = 1$, as in the Mumford-Shah functional for segmentation [19]. For a general $p > 0$, in order to balance the terms and their dimensions in the energy, if d is the unit distance in the $\Omega-$plane, then μ has to be measured in units of $(size\ of\ u_0)^2 \cdot d^{2-p}$, and ν has to be measured in units of $(size\ of\ u_0)^2$.

A different choice for p than in the Mumford-Shah functional, where $p = 1$, to rescale the energy, is to consider directly $p = 2$ (in two dimensions) or $p = \frac{N}{N-1}$ in any dimension $N \geq 2$, from the isoperimetric inequality [9]. We will discuss more this possibility further.

Here, by C we generally mean a hypersurface in $I\!R^N$ and "length(C)" means the Hausdorff $(N-1)$-dimensional measure $\mathcal{H}^{N-1}(C)$.

Therefore, we consider the minimization problem:

$$\inf_{C, c_1, c_2} F(C, c_1, c_2). \tag{5}$$

A. Relation with the Mumford-Shah functional

The Mumford-Shah functional for segmentation is [19]:

$$\begin{aligned} F^{MS}(u, C) \quad = \quad & \mu \cdot \text{length}(C) \\ + \quad & \lambda \int_\Omega |u_0 - u|^2 dx + \int_{\Omega \setminus C} |\nabla u|^2 dx, \end{aligned}$$

where μ, λ are positive parameters. The solution image u obtained by minimizing this functional is formed by smooth regions R_i and with sharp boundaries, denoted here by C.

A reduced form of this problem is simply the restriction of F^{MS} to piecewise constant functions u, i.e. $u = c_i$ with c_i a constant, on each connected component R_i of $\Omega \setminus C$. Therefore, as it was also pointed out by D. Mumford and J. Shah [19], the constants c_i are in fact the averages of u_0 on each R_i. The reduced case is called the minimal partition problem.

Our active contour model for $p = 1$, $\nu = 0$ and $\lambda_1 = \lambda_2 = \lambda$ is a particular case of the minimal partition problem, in which we look for the best approximation u of u_0, as a function taking only two values, namely:

$$u = \begin{cases} \text{average}(u_0) \text{ inside } C \\ \text{average}(u_0) \text{ outside } C, \end{cases} \qquad (6)$$

and with one edge C, represented by the snake or the active contour.

This particular case of the minimal partition problem can be formulated and solved using the level set method [20]. This is presented in the next subsection.

B. The level set formulation of the model

In the rest of this section, we consider the general case in N dimensions, i.e. $x \in \Omega \subset \mathbb{R}^N$ (therefore the word "length" should be replaced by "surface area" and "area" by "volume").

In the level set method [20], C is represented by the zero level set of a Lipschitz function $\phi : \mathbb{R}^N \to \mathbb{R}$, such that

$$\begin{cases} C = \{x \in \mathbb{R}^N : \phi(x) = 0\}, \\ \text{"inside"}(C) = \{x \in \mathbb{R}^N : \phi(x) > 0\} \\ \text{"outside"}(C) = \{x \in \mathbb{R}^N : \phi(x) < 0\}. \end{cases}$$

For the level set formulation of our variational active contour model we follow for instance [28] and [9]. We therefore replace the unknown variable C by the unknown variable ϕ. Using the Heaviside function H and the one-dimensional Dirac measure δ concentrated at 0, defined respectively by:

$$H(z) = \begin{cases} 1, & \text{if } z \geq 0 \\ 0, & \text{if } z < 0, \end{cases}$$

and

$$\delta(z) = \frac{d}{dz} H(z) \text{ (in the sense of distributions)},$$

we express the terms in the energy F in the following way:

$$\text{"length"}\{\phi = 0\} = \int_\Omega |\nabla H(\phi)| = \int_\Omega \delta(\phi)|\nabla \phi|,$$

$$\text{"area"}\{\phi \geq 0\} = \int_\Omega H(\phi) dx,$$

$$\int_{\phi \geq 0} |u_0 - c_1|^2 dx = \int_\Omega |u_0 - c_1|^2 H(\phi) dx,$$

$$\int_{\phi < 0} |u_0 - c_2|^2 dx = \int_\Omega |u_0 - c_2|^2 (1 - H(\phi)) dx.$$

Then the energy $F(\phi, c_1, c_2)$ can be written as:

$$F(\phi, c_1, c_2) = \mu \Big(\int_\Omega |\nabla H(\phi)| \Big)^p + \nu \int_\Omega H(\phi) dx$$

$$+\lambda_1 \int_\Omega |u_0 - c_1|^2 H(\phi) dx + \lambda_2 \int_\Omega |u_0 - c_2|^2 (1 - H(\phi)) dx.$$

Again we recall that in our model, p can have the following values: $p = 1$ for all N, or $p = \frac{N}{N-1}$ for all $N \geq 2$. For the last expression, we are using the isoperimetric inequality (see for instance [9]), which says in some sense that the $\Big(\text{length}(C)\Big)^{\frac{N}{N-1}}$ is "comparable" with the area($insideC$):

$$\int_\Omega H(\phi) dx \leq c \Big(\int_\Omega |\nabla H(\phi)| \Big)^{\frac{N}{N-1}},$$

where c is a constant depending on N only. The level set function ϕ is as before and such that its zero level set in Ω is bounded and of finite length.

We note that, u from (6), solution of our model as a particular case of the Mumford-Shah functional, can simply be written using the level set formulation as: $u = c_1 H(\phi) + c_2(1 - H(\phi))$.

C. The study of the model: existence of minimizers

Let us write the energy $F(\phi, c_1, c_2)$ in the following way:

$$F(\phi, c_1, c_2) = \mu \Big(\int_\Omega \delta(\phi)|\nabla \phi| \Big)^p + \nu \int_\Omega H(\phi) dx$$

$$+\lambda_1 \Big(c_1^2 \int_\Omega H(\phi) dx - 2c_1 \int_\Omega u_0 H(\phi) dx + \int_\Omega u_0^2 H(\phi) dx \Big)$$

$$+\lambda_2 \Big(c_2^2 \int_\Omega (1 - H(\phi)) dx - 2c_2 \int_\Omega u_0 (1 - H(\phi)) dx$$

$$+ \int_\Omega u_0^2 (1 - H(\phi)) dx \Big).$$

Keeping ϕ fixed and minimizing the energy $F(\phi, c_1, c_2)$ with respect to the constants c_1 and c_2,

it is now easy to express these constants function of ϕ by:

$$c_1(\phi) = \frac{\int_\Omega u_0 H(\phi) dx}{\int_\Omega H(\phi) dx} (\text{ average}(u_0) \text{ in } \{\phi \geq 0\}) \quad (7)$$

if $\int_\Omega H(\phi) > 0$ (i.e. if the curve has a nonempty interior in Ω), and

$$c_2(\phi) = \frac{\int_\Omega u_0 (1 - H(\phi)) dx}{\int_\Omega (1 - H(\phi)) dx} (\text{ average}(u_0) \text{ in } \{\phi < 0\}) \quad (8)$$

if $\int_\Omega (1 - H(\phi)) > 0$ (i.e. if the curve has a nonempty exterior in Ω). For the corresponding "degenerate" cases, there are no constrains on the values of c_1 and c_2.

Because the unknown constants c_1 and c_2 have explicit representations as functions of the unknown ϕ, we can consider the energy in ϕ only: $F(\phi, c_1(\phi), c_2(\phi)$. We also remark that, in this case, the energy $F(\phi, c_1(\phi), c_2(\phi))$ can also be expressed as a function of $H(\phi)$ only, which is a characteristic function. Therefore, we can introduce the energy $\mathcal{F}$ depending only on $H(\phi)$, and defined by:

$$\mathcal{F}(H(\phi)) = F(\phi, c_1(\phi), c_2(\phi)), \quad (9)$$

and consider the minimization problem among characteristic functions χ_E, where $E = \{x \in \Omega : \phi(x) \geq 0\}$ and $\chi_E = H(\phi)$:

$$\begin{aligned} \mathcal{F}(\chi_E) &= \mu(\int_\Omega |\nabla \chi_E|)^p + \nu \int_\Omega \chi_E dx \\ &+ \lambda_1 \int_\Omega (u_0 - c_1(\chi_E))^2 \chi_E dx \\ &+ \lambda_2 \int_\Omega (u_0 - c_2(\chi_E))^2 (1 - \chi_E) dx. \end{aligned}$$

Therefore, we obtain the minimization problem:

$$\inf_{\chi_E} \mathcal{F}(\chi_E), \ \chi_E(x) \in \{0, 1\} \ dx - a.e., \quad (10)$$

among characteristic functions of sets E with finite perimeter in Ω, i.e. characteristic functions of bounded variation ([9]).

We expect, of course, to have existence of minimizers of the energy $F(C, c_1, c_2)$, because this is a particular case of the minimal partition problem, for which the existence has been proved for instance in [7]. But because we use a different formulation of our model, the level set method, we prefer to show here existence of minimizers of $\mathcal{F}$ among characteristic functions of sets of finite perimeter (or of bounded variation). This can be done using classical arguments on lower semicontinuous functionals on the BV space.

The functional $\mathcal{F}(\chi_E)$ is well defined on the space $BV(\Omega)$ of functions with bounded variation. We have to consider this space, because the characteristic functions are functions of bounded variation. We need the following *preliminaries* (see [9], [10], [11]): let $\Omega \subset \mathbb{R}^N$ be an open, bounded and connected set. We say that $u \in L^1(\Omega)$ is a function of bounded variation, and we write $u \in BV(\Omega)$, if its distributional derivative $Du = (D_1 u, ..., D_N u)$ is a vector measure with bounded total variation, i.e. if:

$$|Du|(\Omega)$$

$$= \sup_f \Big\{ \int_\Omega u \text{div} f dx | f \in C_c^1(\Omega; \mathbb{R}^N), |f| \leq 1 \Big\} < \infty.$$

A particular case of functions of bounded variation are the characteristic functions of sets of finite perimeter: if E is a set in $\mathbb{R}^N$, then the perimeter of E in Ω is $\text{per}_\Omega(E) := \int_\Omega |\nabla \chi_E|$ and E has finite perimeter in Ω if and only if $\chi_E \in BV(\Omega)$.

The space $BV(\Omega)$ is a Banach space, endowed with the norm:

$$\|u\|_{BV(\Omega)} = \|u\|_{L^1(\Omega)} + |Du|(\Omega).$$

Assume further that $\partial\Omega$ is Lipschitz. Then we have the following basic result (see for instance [9]): if $(u_n)_{n \geq 1}$ is a bounded sequence in $BV(\Omega)$, then there exists a subsequence (u_{n_j}) of (u_n) and a function $u \in BV(\Omega)$, such that $u_{n_j} \to u$ strongly in $L^1(\Omega)$, as $n_j \to \infty$, and

$$|Du|(\Omega) \leq \liminf_{n_j \to \infty} |Du_{n_j}|(\Omega).$$

We state now our existence result (assume $\mu > 0$, λ_1, λ_2, $\nu \geq 0$):

Theorem 1: If $u_0 \in L^\infty(\Omega)$, then the following minimization problem

$$\inf_{\chi_E} \mathcal{F}(\chi_E), \ \chi_E \in BV(\Omega), \ \chi_E(x) \in \{0, 1\} \ dx - \text{a.e.},$$

has a solution.

Proof. Let $(\chi_{E_n})_{n \geq 1}$ be a minimizing sequence of $\mathcal{F}$, i.e.

$$\inf_{\chi_E} \mathcal{F}(\chi_E) = \lim_{n \to \infty} \mathcal{F}(\chi_{E_n}).$$

Then there is a constant $M > 0$ s.t. $|\nabla \chi_{E_n}|(\Omega) \leq M$, for all $n \geq 1$. Of course, $0 \leq \chi_{E_n} \leq 1$, $dx - a.e.$ in Ω; hence $\|\chi_{E_n}\|_{L^1(\Omega)} \leq |\Omega|$, for all $n \geq 1$ (we have to justify this bound in the case when we do not consider the

area term in the functional, i.e. when $\nu = 0$). Then the sequence χ_{E_n} is bounded in $BV(\Omega)$. Therefore, there is a subsequence $(\chi_{E_{n_j}})$ of (χ_{E_n}), $j \geq 1$, and a function $u \in BV(\Omega)$ such that $\chi_{E_{n_j}} \rightarrow u$ strongly in $L^1(\Omega)$. Then for a subsequence, still denoted E_{n_j}, $\chi_{E_{n_j}} \rightarrow u$ dx-a.e. in Ω. We therefore deduce that $u = \chi_E$, $dx-$a.e., where E has finite perimeter in Ω.

By the previous lower semi-continuity result, we have:

$$\Big(\int_\Omega |\nabla \chi_E|\Big)^p \leq \liminf_{n_j \rightarrow \infty} \Big(\int_\Omega |\nabla \chi_{E_{n_j}}|\Big)^p.$$

It is easy to show the continuity or the lower semi-continuity in $L^1(\Omega)$ of the fitting energy. For instance, if $\int_\Omega \chi_E dx > 0$, under the usual assumption for images that $u_0 \in L^\infty(\Omega)$, all the integrals depending on $\chi_{E_{n_j}}$ converge (strongly) to the corresponding integrals depending on χ_E. The same remains true if we have $1 - \chi_E$ instead of χ_E. For instance, in the "degenerate" case when $\int_\Omega \chi_E dx = 0$, then the first term of the fitting energy is zero, and obviously the lower semi-continuity inequality will be satisfied, because the corresponding term in $\chi_{E_{n_j}}$ is positive or zero.

Finally, we have:

$$\mathcal{F}(\chi_E) \leq \liminf_{n_j \rightarrow \infty} \mathcal{F}(\chi_{E_{n_j}}),$$

by the above lower semi-continuity property of the total variation and the strong convergence in $L^1(\Omega)$ of the other terms. Then χ_E is a minimizer of $\mathcal{F}$ among characteristic functions of sets of finite perimeter in Ω. ∎

Once χ_E is obtained, using $\chi_E = H(\phi)$, c_1 and c_2 are uniquely determined by (7) and (8) (except in the "degenerate" cases). The level set function ϕ is used only to represent the snake and has many numerical advantages, but the problem could also be formulated and solved only in terms of characteristic functions.

D. The Euler-Lagrange equations

In order to compute the associated Euler-Lagrange equation for the unknown function ϕ, we have to consider slightly regularized versions of the functions H and δ, denoted here by H_ε and δ_ε, such that $\delta_\varepsilon = H'_\varepsilon$. For the moment, let H_ε be any $C^2(\overline{\Omega})$ regularization of H, and $\delta_\varepsilon = H'_\varepsilon$. We will give further examples of such approximations.

The associated regularized functional F_ε of F will therefore be:

$$F_\varepsilon(\phi, c_1, c_2) = \mu\Big(\int_\Omega \delta_\varepsilon(\phi)|\nabla\phi| dx\Big)^p + \nu \int_\Omega H_\varepsilon(\phi) dx$$
$$+\lambda_1 \int_\Omega |u_0 - c_1|^2 H_\varepsilon(\phi) dx + \lambda_2 \int_\Omega |u_0 - c_2|^2 (1 - H_\varepsilon(\phi)) dx,$$

and we consider the following regularized minimization problem:

$$\inf_{\phi, c_1, c_2} F_\varepsilon(\phi, c_1, c_2). \tag{11}$$

Keeping c_1 and c_2 fixed, and minimizing F_ε with respect to ϕ, we have the following relations, choosing ψ as a test function of the same type as ϕ:

$$\lim_{t \rightarrow 0} \frac{1}{t}\Big(F_\varepsilon(\phi + t\psi, c_1, c_2) - F_\varepsilon(\phi, c_1, c_2)\Big) =$$
$$p\Big(\int_\Omega \delta_\varepsilon(\phi)|\nabla\phi| dx\Big)^{p-1}$$
$$\cdot \int_\Omega \mu\Big(\delta'_\varepsilon(\phi)|\nabla\phi|\psi + \delta_\varepsilon(\phi)\frac{\nabla\phi\nabla\psi}{|\nabla\phi|}\Big) dx$$
$$+ \int_\Omega \delta_\varepsilon(\phi)(\nu + \lambda_1(u_0 - c_1)^2 - \lambda_2(u_0 - c_2)^2)\psi dx = 0.$$

Integrating by parts and using Green's theorem, we obtain

$$p\Big(\int_\Omega \delta_\varepsilon(\phi)|\nabla\phi| dx\Big)^{p-1}\Big(\int_\Omega \mu\delta'_\varepsilon(\phi)|\nabla\phi|\psi dx$$
$$+ \int_{\partial\Omega} \mu\frac{\delta_\varepsilon(\phi)}{|\nabla\phi|}\frac{\partial\phi}{\partial n}\psi ds - \int_\Omega \mu\nabla\Big(\delta_\varepsilon(\phi)\frac{\nabla\phi}{|\nabla\phi|}\Big)\psi dx\Big)$$
$$+ \int_\Omega \delta_\varepsilon(\phi)(\nu + \lambda_1(u_0 - c_1)^2 - \lambda_2(u_0 - c_2)^2)\psi dx = 0.$$

Formally developing the divergence operator, we finally obtain:

$$p\Big(\int_\Omega \delta_\varepsilon(\phi)|\nabla\phi| dx\Big)^{p-1}\Big(-\int_\Omega \mu\delta_\varepsilon(\phi)\nabla\Big(\frac{\nabla\phi}{|\nabla\phi|}\Big)\psi dx$$
$$+ \int_{\partial\Omega} \mu\frac{\delta_\varepsilon(\phi)}{|\nabla\phi|}\frac{\partial\phi}{\partial n}\psi ds\Big)$$
$$+ \int_\Omega \delta_\varepsilon(\phi)(\nu + \lambda_1(u_0 - c_1)^2 - \lambda_2(u_0 - c_2)^2)\psi dx = 0,$$

for all test functions ψ. Choosing first $\psi \in C_c^1(\Omega)$, and secondly zero in Ω and non-zero in $\partial\Omega$, we deduce the following Euler-Lagrange equation for ϕ:

$$\begin{cases} \delta_\varepsilon(\phi)\Big[\mu p\Big(\int_\Omega \delta_\varepsilon(\phi)|\nabla\phi|\Big)^{p-1}\mathrm{div}\Big(\frac{\nabla\phi}{|\nabla\phi|}\Big) - \nu \\ -\lambda_1(u_0 - c_1)^2 + \lambda_2(u_0 - c_2)^2\Big] = 0 \text{ in } \Omega, \\ p\Big(\int_\Omega \delta_\varepsilon(\phi)|\nabla\phi|\Big)^{p-1}\frac{\delta_\varepsilon(\phi)}{|\nabla\phi|}\frac{\partial\phi}{\partial n} = 0 \text{ on } \partial\Omega. \end{cases}$$

Recall that the expression $K(\phi) = -\mathrm{div}\Big(\frac{\nabla\phi}{|\nabla\phi|}\Big)$ denotes the curvature of the zero-level front.

E. Regularizations of H and δ

First possible regularizations by $C^2(\overline{\Omega})$ and respectively $C^1(\overline{\Omega})$ functions, as proposed for instance in [28], are:

$$H_{1,\varepsilon}(z) = \begin{cases} 1 \text{ if } z > \varepsilon \\ 0 \text{ if } z < -\varepsilon \\ \frac{1}{2}\Big[1 + \frac{z}{\varepsilon} + \frac{1}{\pi}\sin\Big(\frac{\pi z}{\varepsilon}\Big)\Big] \text{ if } |z| \le \varepsilon \end{cases}$$

and

$$\delta_{1,\varepsilon}(z) = H'_{1,\varepsilon}(z) = \begin{cases} 0 \text{ if } |z| > \varepsilon \\ \frac{1}{2\varepsilon}\Big[1 + \cos\Big(\frac{\pi z}{\varepsilon}\Big)\Big], \text{ if } |z| \le \varepsilon. \end{cases}$$

In this paper, we introduce and use in our experiments (see further) the following $C^\infty(\overline{\Omega})$ regularized versions of H and δ, defined by:

$$H_{2,\varepsilon}(z) = \frac{1}{2}(1 + \frac{2}{\pi}\arctan(\frac{z}{\varepsilon})),$$

$$\delta_{2,\varepsilon}(z) = H'_{2,\varepsilon}(z) = \frac{1}{\pi}\cdot\frac{\varepsilon}{\varepsilon^2 + z^2}.$$

These distinct approximations and regularizations of the functions H and δ are presented in Figure 2.

As $\varepsilon \to 0$, both approximations converge to H and δ. A difference is that $\delta_{1,\varepsilon}$ has small compact support, the interval $[-\varepsilon, \varepsilon]$, while $\delta_{2,\varepsilon}$ is different of zero everywhere.

Because our energy is non-convex (allowing therefore many local minima), and because $\delta_{1,\varepsilon}$ has a very small compact support, the interval $[-\varepsilon, \varepsilon]$, the numerical algorithm may depend on the initial curve, and will not necessarily compute a global minimizer. In some of our tests using the first approximation, we obtained only a local minimizer of the energy. Using the second approximations, the algorithm has the tendency to compute a global minimizer. One of the reasons is that the Euler-Lagrange equation for ϕ acts only locally, on a few level curves arround $\phi = 0$ using the first approximation, while by the second approximation, the equation acts on all level curves, of course stronger on the zero level curve, but not only locally. In this way, in practice, we can obtain a global minimizer, independently of the position of the initial curve, and this allow to automatically detect interior contours (see Section 4).

We mention that, in order to extend the evolution to all level sets of ϕ, another possibility is to replace $\delta(\phi)$ by $|\nabla\phi|$ (see [28]). In our paper, we would like to keep $\delta(\phi)$ in the equation, to remain close the the initial minimization problem. The problem of extending

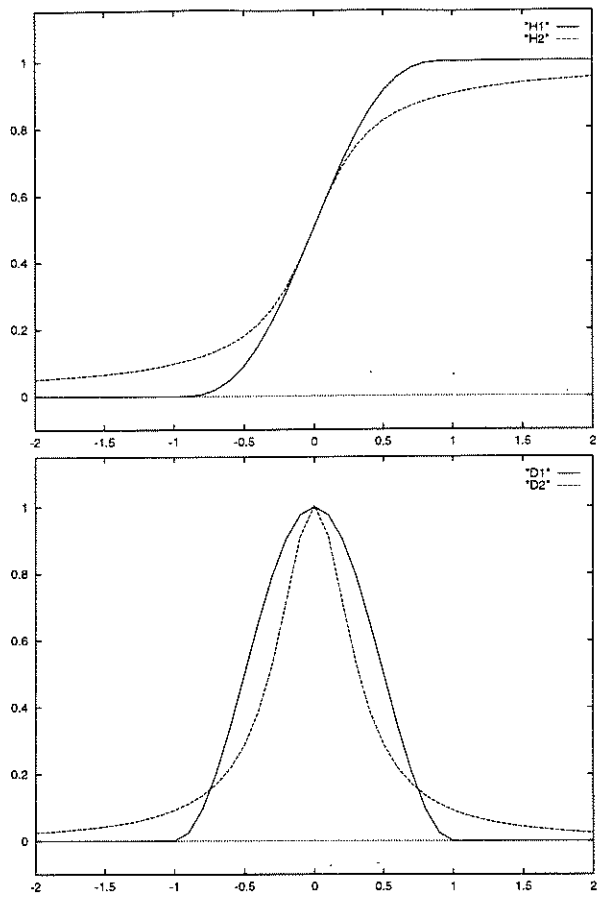

Fig. 2. The two different regularizations of the Heaviside function (top) and Delta function (bottom).

the evolution to all level sets of ϕ was solved here using the aproximation $\delta_{2,\varepsilon}$of the Dirac δ function, which is different of zero everywere.

For other approximations of the Dirac δ function, we refer the reader for instance to [3].

III. The numerical approximation of the model

To discretize the equation in ϕ, we use a finite differences implicit scheme and we denote here the space variable by $(x, y) \in \Omega \subset I\!R^2$ $(N = 2)$. We also parametrize the descent direction by an artificial time. The new evolution problem is:

$$\begin{cases} c_1(\phi) = \frac{\int_\Omega u_0 H_\varepsilon(\phi)dxdy}{\int_\Omega H_\varepsilon(\phi)dxdy}, \quad c_2(\phi) = \frac{\int_\Omega u_0(1-H_\varepsilon(\phi))dxdy}{\int_\Omega(1-H_\varepsilon(\phi))dxdy} \\ \frac{\partial\phi}{\partial t} = \delta_\varepsilon(\phi)\Big[\mu p\Big(\int_\Omega \delta_\varepsilon(\phi)|\nabla\phi|\Big)^{p-1}\operatorname{div}\Big(\frac{\nabla\phi}{|\nabla\phi|}\Big) - \nu \\ -\lambda_1(u_0 - c_1)^2 + \lambda_2(u_0 - c_2)^2\Big] \text{ in } \Omega, \\ \phi(t, x, y) = \phi_0(x, y) \text{ in } \Omega, \\ p\Big(\int_\Omega \delta_\varepsilon(\phi)|\nabla\phi|\Big)^{p-1}\frac{\delta_\varepsilon(\phi)}{|\nabla\phi|}\frac{\partial\phi}{\partial n} = 0 \text{ on } \partial\Omega. \end{cases} \tag{12}$$

We recall here the usual notations for finite differences: let h be the step space, and $(x_i, y_j) = (ih, jh)$ be the grid points, for $1 \leq i, j \leq M$. Let $\phi^n_{i,j} = \phi(n \triangle t, x_i, y_j)$ be an approximation of $\phi(t, x, y)$ depending on h, with $n \geq 0$, $\phi^0 = \phi_0$. The finite differences are:

$$\triangle^x_- \phi_{i,j} = \phi_{i,j} - \phi_{i-1,j},\ \triangle^x_+ \phi_{i,j} = \phi_{i+1,j} - \phi_{i,j},$$
$$\triangle^y_- \phi_{i,j} = \phi_{i,j} - \phi_{i,j-1},\ \triangle^y_+ \phi_{i,j} = \phi_{i,j+1} - \phi_{i,j}.$$

The algorithm is as follows (we essentially adopt the method from [24] for the discretization of the divergence operator and the iterative algorithm from [2]): knowing ϕ^n, we first compute $c_1(\phi^n)$ and $c_2(\phi^n)$ using (12), and length$\{\phi^n = 0\} = \int_\Omega \delta_h(\phi^n)|\nabla \phi^n| dxdy$, denoted by $L(\phi^n)$. Then, we compute ϕ^{n+1} by the following discretization and linearization of the equation in ϕ:

$$\frac{\phi^{n+1}_{i,j} - \phi^n_{i,j}}{\triangle t} = \delta_h(\phi^n_{i,j})\Big[\frac{\mu}{h^2}(p \cdot L(\phi^n)^{p-1})$$

$$\triangle^x_- \Big(\frac{\triangle^x_+ \phi^{n+1}_{i,j}}{\sqrt{(\triangle^x_+ \phi^n_{i,j})^2/(h^2) + (\phi^n_{i,j+1} - \phi^n_{i,j-1})^2/(2h)^2}}\Big)$$

$$+\frac{\mu}{h^2}(p \cdot L(\phi^n)^{p-1})$$

$$\triangle^y_- \Big(\frac{\triangle^y_+ \phi^{n+1}_{i,j}}{\sqrt{(\phi^n_{i+1,j} - \phi^n_{i-1,j})^2/(2h)^2 + (\triangle^y_+ \phi^n_{i,j})^2/(h^2)}}\Big)$$

$$-\nu - \lambda_1(u_{0,i,j} - c_1(\phi^n))^2 + \lambda_2(u_{0,i,j} - c_2(\phi^n))^2\Big].$$

Denoting by C_1, C_2 , C_3 and C_4 the coefficients of $\phi^{n+1}_{i+1,j}$, $\phi^{n+1}_{i-1,j}$, $\phi^{n+1}_{i,j+1}$ and $\phi^{n+1}_{i,j-1}$ respectively, ϕ^{n+1} will be the unique fixed point of the following linear system:

$$\phi^{n+1}_{i,j}\Big[1 + \tfrac{\mu(p \cdot L(\phi^n)^{p-1})\delta_h(\phi^n_{i,j})}{h^2}(C_1 + C_2 + C_3 + C_4)\Big]$$

$$= \phi^n_{i,j} + \triangle t \delta_h(\phi^n_{i,j})\Big[\tfrac{\mu}{h^2}(p \cdot L(\phi^n)^{p-1})$$

$$(C_1\phi^{n+1}_{i+1,j} + C_2\phi^{n+1}_{i-1,j} + C_3\phi^{n+1}_{i,j+1} + C_4\phi^{n+1}_{i,j-1})$$

$$-\nu - \lambda_1(u_{0,i,j} - c_1(\phi^n))^2 + \lambda_2(u_{0,i,j} - c_2(\phi^n))^2\Big].$$

This linear system is solved by an iterative method, and for more details, we refer the reader to [2].

We also need at each step to reinitialize ϕ to be the signed distance function to its zero-level curve, because we work with the regularized function δ_ε. This procedure is standard (see [26] and [28]), and prevents the level set function to become too flat, or it can be seen as a rescaling.

This reinitialization procedure is made by the following evolution equation [26]:

$$\begin{cases} \psi_\tau = sign(\phi(t))(1 - |\nabla \psi|) \\ \psi(0, \cdot) = \phi(t, \cdot), \end{cases} \tag{13}$$

where $\phi(t, \cdot)$ is our solution ϕ at time t. Then the new $\phi(t, \cdot)$ will be ψ, such that ψ is obtained at the steady state of (13). We need to do the reinitialization at each iteration, but only few iterations are necessarily to solve (13), in order to have the signed distance function near the front. The solution $\psi(t, \cdot)$ of (13) will have the same zero-level set as $\phi(t, \cdot)$ and away from this set, $|\nabla \psi|$ will converge to 1. To discretize the equation (13), we use the following scheme (see [23] and [26]):

$$\psi^{\eta+1}_{i,j} = \psi^\eta_{i,j} - \triangle \tau \text{sign}(\phi(t))G(\psi^\eta_{i,j}),$$

where the flux $G(\psi^\eta_{i,j})$ is defined as follows: using the notations

$$a = (\triangle^x_- \psi_{i,j})/h = (\psi_{i,j} - \psi_{i-1,j})/h,$$
$$b = (\triangle^x_+ \psi_{i,j})/h = (\psi_{i+1,j} - \psi_{i,j})/h,$$
$$c = (\triangle^y_- \psi_{i,j})/h = (\psi_{i,j} - \psi_{i,j-1})/h,$$
$$d = (\triangle^y_+ \psi_{i,j})/h = (\psi_{i,j+1} - \psi_{i,j})/h,$$

the flux G is

$$G(\psi_{i,j}) = \begin{cases} \sqrt{\max((a^+)^2, (b^-)^2) + \max((c^+)^2, (d^-)^2)} \\ -1, \text{ if } \phi(t, x_i, y_j) > 0, \\ \sqrt{\max((a^-)^2, (b^+)^2) + \max((c^-)^2, (d^+)^2)} \\ -1, \text{ if } \phi(t, x_i, y_j) < 0, \\ 0, \text{ otherwise,} \end{cases}$$

where $a^+ = \max(a, 0)$, $a^- = \min(a, 0)$, and so on.

In practice, to not perform more iterations than necessarily, we can check whether the solution is stationary, computing each time the quantity [28]:

$$Q = \frac{\sum_{|\phi^m_{i,j}| < h} |\phi^{m+1}_{i,j} - \phi^m_{i,j}|}{M},$$

where M is the number of grid points where $|\phi^m_{i,j}| < h$. Recall that h denotes the step space. If $Q \leq (\triangle t)(h^2)$, then the solution is stationary and we stop, else we continue the algorithm.

Finally, the principal steps of our algorithm are:

- Initialize ϕ^0 by ϕ_0, $n = 0$.
- Compute $c_1(\phi^n)$ and $c_2(\phi^n)$ using (12), and length$\{\phi^n = 0\} = L(\phi^n)$ if $p = 2$.

- Solve the PDE in ϕ from (12), to obtain ϕ^{n+1}.
- Reinitialize: replace ϕ^{n+1} by the signed distance function to $\{\phi^{n+1} = 0\}$.
- Check wether the solution is stationary near the front. If not, $n = n + 1$ and repeat.

In our numerical results, we make one iteration for each step. Only if the image is noisy (like in Fig. 3), we perform 5 iterations to compute ϕ^{n+1} and the distance function, for each fixed $c_1(\phi^n)$ and $c_2(\phi^n)$. For the case $p = 2$, length$\{\phi = 0\} = L(\phi^n)$ is updated at each iteration in ϕ.

IV. Experimental results

We end the paper by presenting numerical results using our model on various synthetic and real images, with different types of contours and shapes. We show the active contour evolving in the original image u_0, and in some examples, we also show the piecewise-constant approximation or segmentation of u_0 (given by the averages c_1 and c_2). In all our numerical results we use the second approximations H_2 and δ_2 of the Heaviside and Dirac delta functions, in order to automatically detect interior contours. Also, $p = 1$ everywhere, except for Fig. 13, were $p = 2$.

We first consider images with classical contours with gradient.

In Fig. 3 we show how our model works on a noisy synthetic image, with different shapes, convexities and an interior contour, which is automatically detected, without considering a second initial curve (here $\mu > 0$, $\nu = 0$, $\lambda_1 = \lambda_2$).

In Fig. 4, we show that our model can detect different objects of different intensities, and with blurred boundaries. In this case, we needed to use $\lambda_1 < \lambda_2$, and $\mu > 0$, $\nu = 0$. Again, the interior contour of the torus is automaticaly detected, without considering a second initial curve. This is also due to the fact that the velocity has a global dependence, and the curve is automatically attracted toward the objects. In this example we also show that the initial curve does not necessarily surround the objects.

In Fig. 5 we show how we can detect lines and curves (not necessarily closed) in a noisy image. The final level set function is zero on the curves and negative outside the curves.

In the next examples (Fig. 6, 7, 8 and 9), we consider images with "contours without gradients" or "cognitive contours" (see [12]). We also illustrate here the role of the length term as a scale parameter: if μ is small or even zero, then any small objects are detected; if μ is large, then only larger objects are detected, or objects formed by grouping by resemblance.

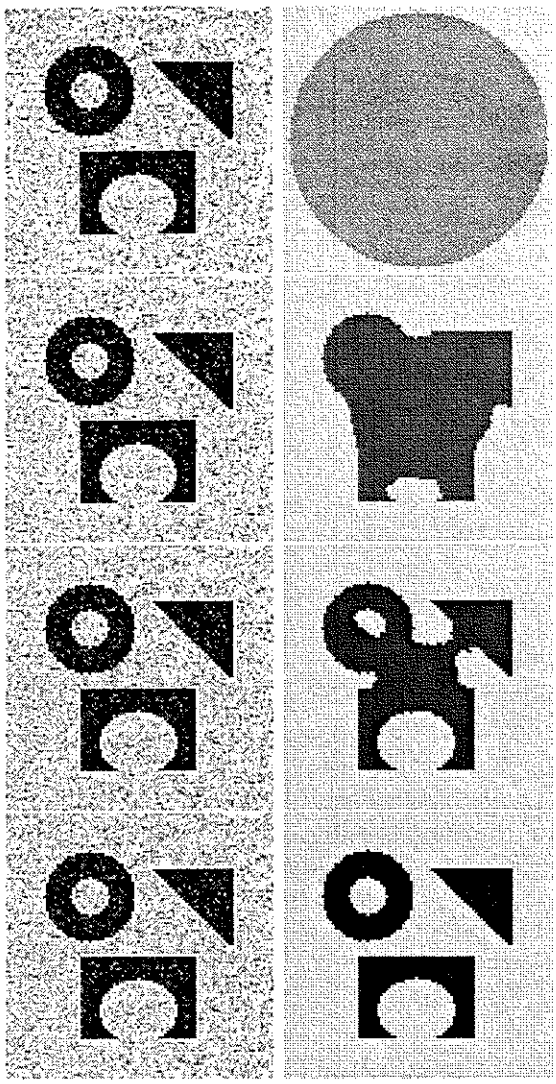

Fig. 3. Detection of different objects from a very noisy image, with various convexities and with an interior contour which is automatically detected, using only one initial curve. After a short time, an interior contour appears inside the torus, and then expands. Left: u_0 and the contour. Right: the piecewise constant approximation of u_0.

In Fig. 6 top, without the length term ($\mu = 0$), all circles are detected as independent objects. With more weight on length term (i.e. a large μ), in Fig. 6, bottom, we show that our algorithm can detect objects defined by grouping according to Kanizsa's "proximity rule".

In Fig. 7 we show how the grouping is based on the chromatic ressemblance or identity, among objects of the same shape.

In Fig. 8 we validate our model on a very different problem: to detect features in spatial point processes

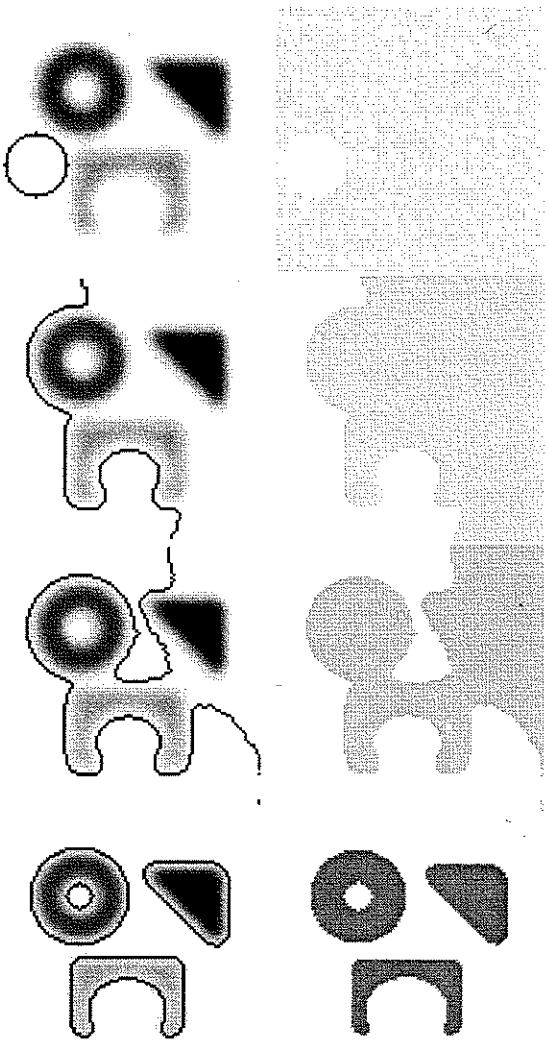

Fig. 4. Detection of blurred objects and with different intensities. Here, the term in the functional which measures the average between the image and the constant c_1 inside the curve is less important than on the outside ($\lambda_1 < \lambda_2$). Also, the initial curve can start everywhere in the image (the choice for the signes of ϕ inside and outside the curve is not important).

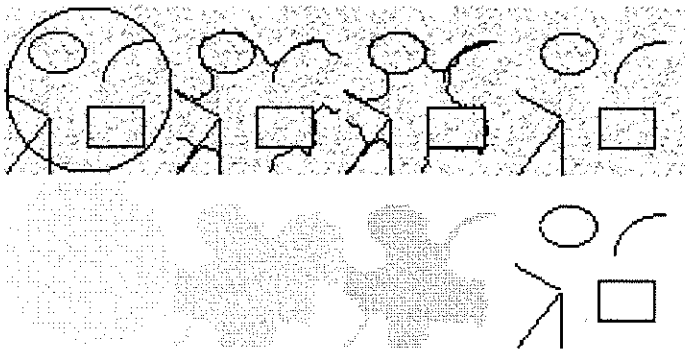

Fig. 5. Detection of lines and curves not necessarily closed.

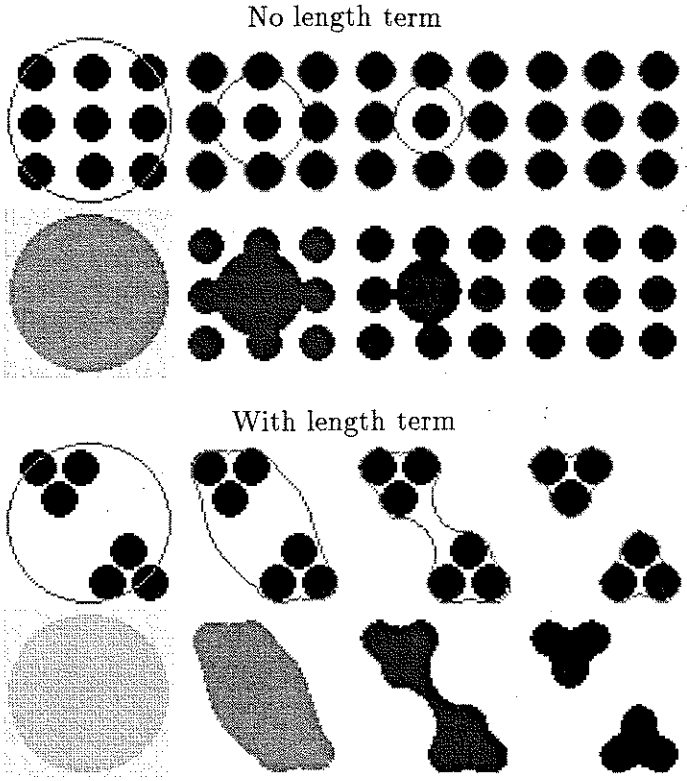

Fig. 6. Results showing the role of the length term and of μ as a scale parameter. Top: $\mu = 0$ (no constraint on the length of the curve). Bottom: $\mu > 0$ is large (important constraint on the length of the curve).

in the presence of substantial cluster. One application is the detection of minefields using reconnaissance aircraft images that identify many objects that are not mines. These problems are usualy solved using statistical methods (see for instance [8] and [4]). By this application, we show again how our model can be used to detect objects or features whith contours without gradient. This is not possible using classical snakes or active contours based on the gradient.

A similar application is presented in Fig. 9, where the white points are Europe nightlights.

We next consider an image with very smooth contours. In Fig. 10 left, we show results obtained using our model, while in Fig. 10 right, we show the results obtained with a classical active contour model based on the edge-function $g(|\nabla u_0|)$ (here the geometric model), by which the curve cannot detect the smooth boundary.

We also show examples of real noisy/blurred images, with different types of contours or shapes, illustrating all the advantages of our model: the ability of detecting smooth boundaries, scale adaptivity and automatic change of topology.

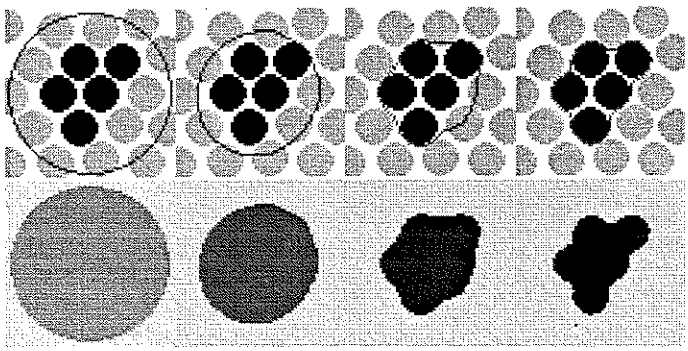

Fig. 7. Contour without gradient. The detected large "object" is a "grouping" of smaller objects of the same color (grouping by chromatic resemblance or identity).

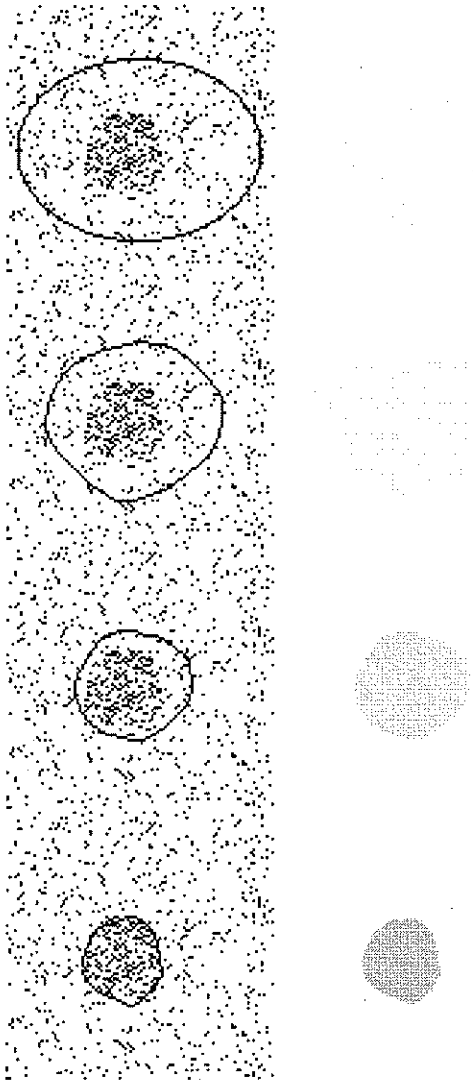

Fig. 8. Detection of a simulated minefield, with contour without gradient.

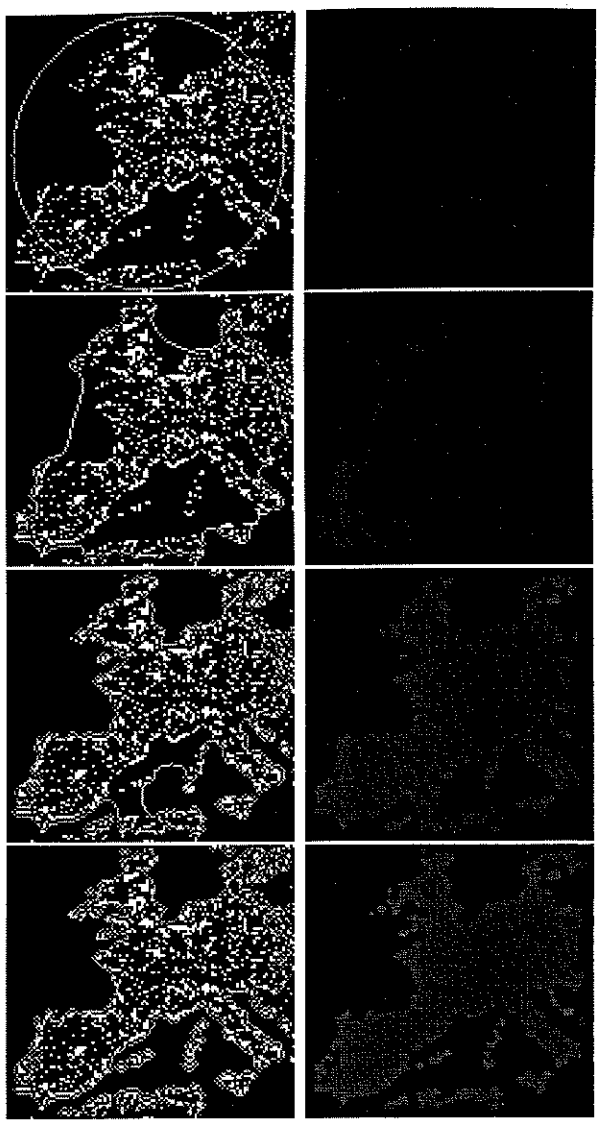

Fig. 9. Europe nightlights.

In Figures 11 and 12 we detect the contours of two galaxies.

In Fig. 13, we consider an art picture from Los Angeles Times, by Brian Forrest. Here, $p = 2$ (we have the square of the length term in the energy) and the initial curve is the boundary of the image. After a time, a curve in the middle of the image appears and expands until merges with the initial evolving curve.

In Fig. 14 we show how the tumor is detected from an MRI image (here $\mu > 0$, $\nu > 0$, $\lambda_1 = \lambda_2$). Note that we use the area term in addition, to force the initial curve to move only "inside".

Finally, in Fig. 15, the algorithm detects the contours of a plane from a real noisy image ($\mu > 0$, $\lambda_1 = \lambda_2$).

Of course that our model has its limitations. For instance, it will be interesting to extend the model to

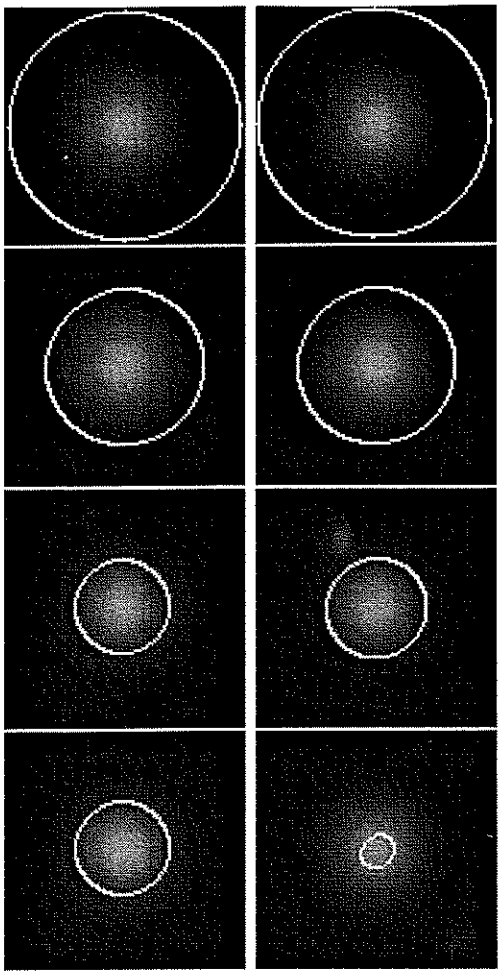

Fig. 10. Left: detection of an object whith a very smooth contour using our model without edge-function. Right: results on the same image using the geometric model "with gradient" (2). The object is not detected.

the general case of the Mumford-Shah functional.

On the other side, there are objects which cannot be detected using the intensity average only. For instance, we show in Fig. 16 (top and middle), two such examples, together with the averages inside and outside the supposed objects, which are practically the same.

One way to overcome this difficulty, would be to use other informations from the initial image u_0, like the curvature (see Fig. 17 left), or the orientation of level sets (see Fig. 17 right). In this framework, we refer the reader to [15].

In the next results, we replaced in our model u_0 by $curv(u_0)$ (Fig. 18) and by $orientation(u_0)$ (Fig. 19, where we considered the angle of the normal to the level curves). Other discriminants may be considered.

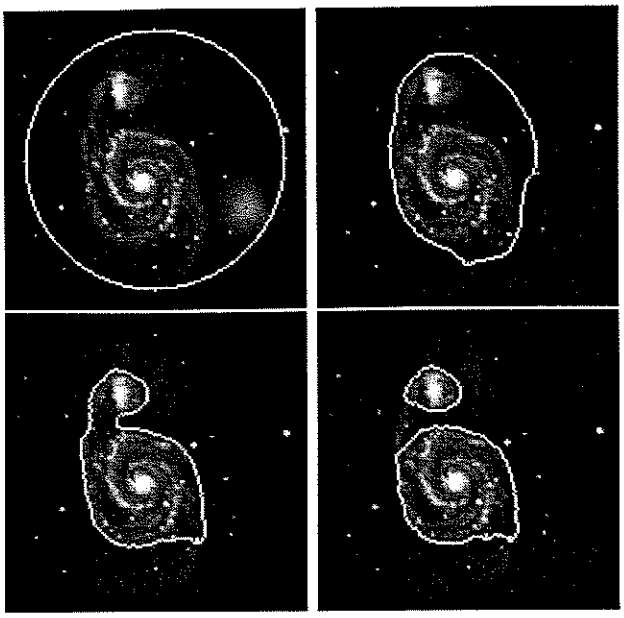

Fig. 11. Detection of the contours of a galaxie.

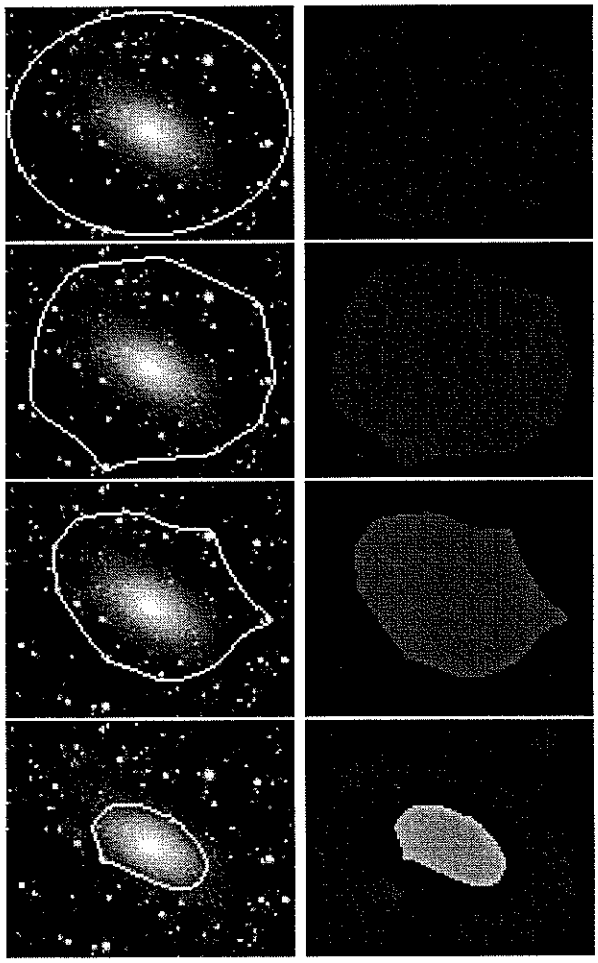

Fig. 12. Real image: a galaxie with smooth boundaries.

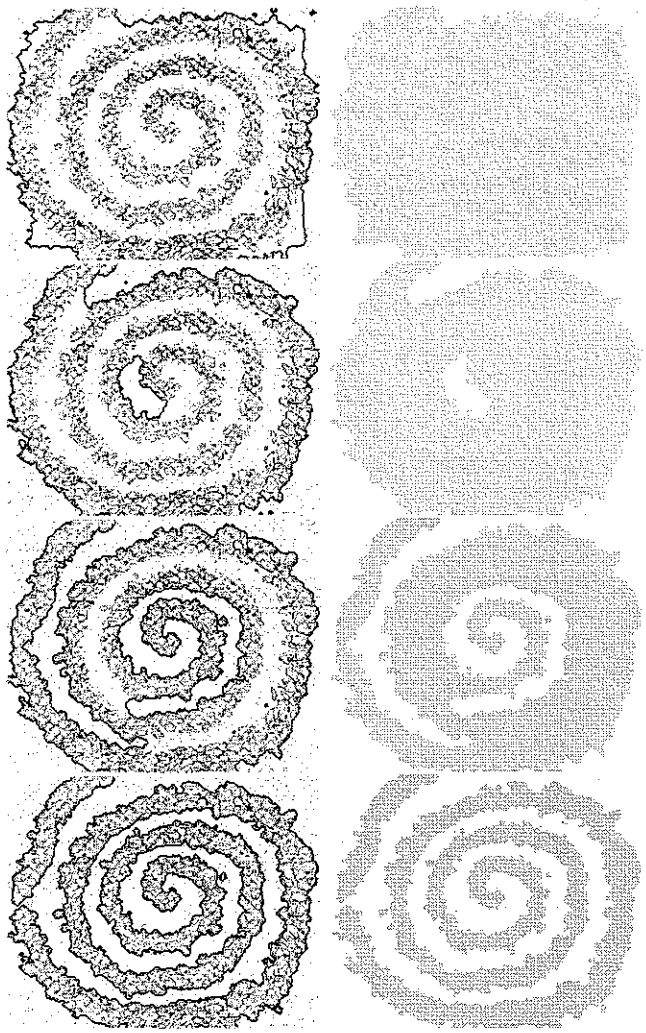

Fig. 13. A spiral, from an art picture.

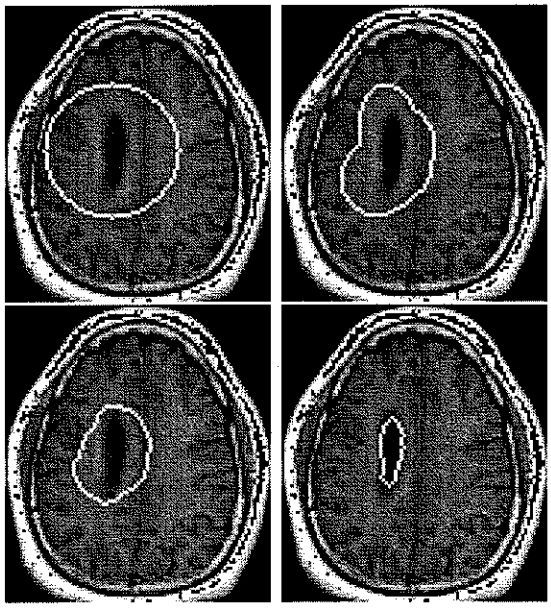

Fig. 14. Detection of a tumor in a MRI image.

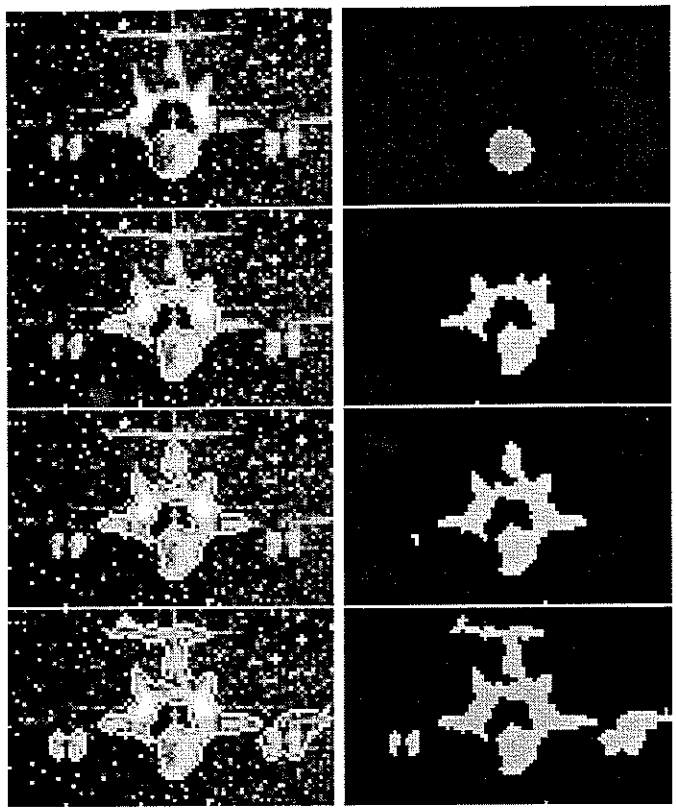

Fig. 15. Detection of the contours of a plane from a noisy image.

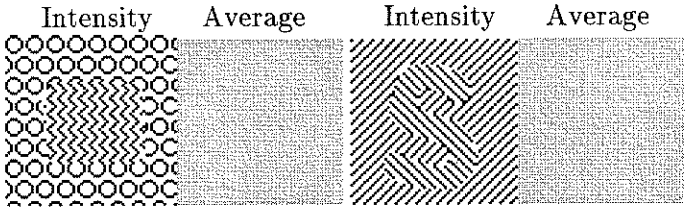

Fig. 16. Examples of images for which the averages "inside" and "outside" the objects are the same.

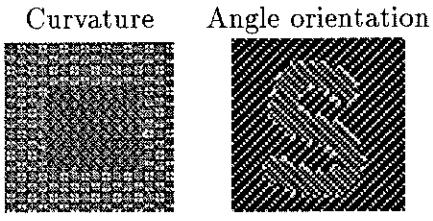

Fig. 17. Left: image curvature of Fig. 16 left. Right: image angle of the orientation of level sets, from Fig. 16 right.

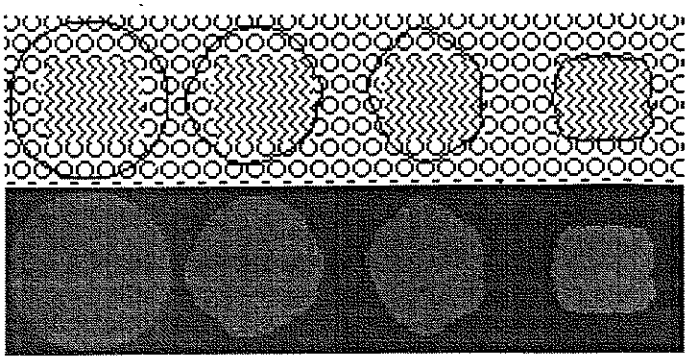

Fig. 18. Detection of an object without gradient, formed by grouping based on shape identity. In our model, we replaced u_0 from Fig. 16 left, by curv(u_0) (Fig. 17 left).

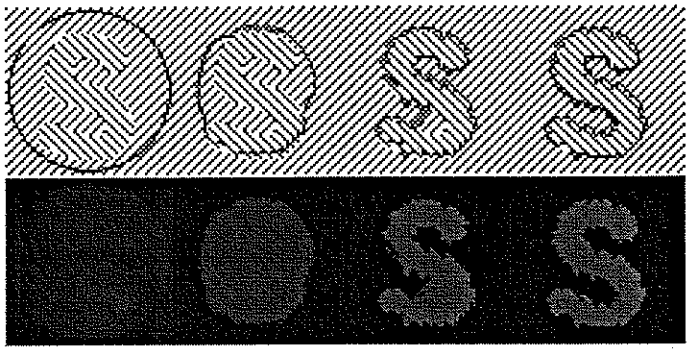

Fig. 19. Similar example, with object without gradient (here the grouping is based on orientation identity). In our model, we replaced u_0 from Fig. 16 right, by the "image angle" (Fig. 17 right) of the normal of level curves of u_0.

V. Concluding remarks and discussions

In this paper we proposed an active contour model based on Mumford-Shah segmentation techniques and level set methods. Our model is not based on an edge-function to stop the evolving curve on the desired boundary. Also, we do not need to smooth the initial image, even if it is very noisy and in this way, the locations of boundaries are very well detected and preserved. By our model, we can detect objects whose boundaries are not necessarily defined by gradient or with very smooth boundaries, for which the classical active contour models are not aplicable. Finally, we can automatically detect interior contours starting with only one initial curve. The position of the initial curve can be anywhere in the image, and not necessarily arround the objects to be detected. We validated our model by various numerical results.

ACKNOWLEDGEMENTS

The authors would like to thank Jean-Michel Morel and Guillermo Sapiro for suggesting us the refferences on Kanisza's work ([12]) and Paragios-Deriche work respectively ([21], [22]), to Michael J. Black and Steve Ruuth for valuable conversations, and especially to Stanley Osher for the very usefull discussions in the "level set collective".

References

[1] G. Aubert and L. Blanc-Féraud, *An elementary proof of the equivalence between 2D and 3D classical snakes and geodesic active contours*, INRIA Rapport de Recherche 3340, Janvier 1998.

[2] G. Aubert and L. Vese, *A variational method in image recovery*, SIAM J. Num. Anal., 34/5(1997), pp. 1948-1979.

[3] R. P. Beyer and R. J. Leveque, *Analysis of a one-dimensional model for the immersed boundary method*, SIAM J. Numer. Anal. Vol. 29, No 2, pp. 332-364, April 1992.

[4] S. Byers and A. Raftery, *Nearest-Neighbor Clutter Removal for Estimating Features in Spatial Point Processes*, Journal of the American Statistical Association, June 1998, Vol. 93, No. 442, Theory and Methods, pp. 577-584.

[5] V. Caselles, F. Catté, T. Coll and F. Dibos, *A geometric model for active contours in image processing*, Numerische Mathematik 66, 1993, pp. 1-31.

[6] V. Caselles, R. Kimmel, and G. Sapiro, *On geodesic active contours*, Int. Journal of Computer Vision, 22(1), 1997, pp. 61-79.

[7] G. Dal Maso, J.M. Morel, and S. Solimini, *A variational method in image segmentation: existence and approximation results*, Acta Matematica, Vol. 168, 89-151, 1992.

[8] A. Dasgupta and A. Raftery, *Detecting Features in Spatial Point Processes With Clustter via Model-Based Clustering*, Journal of the American Statistical Association, March 1998, Vol. 93, No. 441, Theory and Methods, pp. 294-302.

[9] L. C. Evans and R. F. Gariepy, *Measure Theory and Fine Properties of Functions*, CRC Press, 1992.

[10] H. Federer, *Geometric measure theory*, Berlin, Heidelberg, New-York: Springer-Verlag, 1969.

[11] E. Giusti, *Minimal surfaces and functions of bounded variation*, Basel, Boston, Stuttgart: Birkhäuser Verlag, 1984.

[12] G. Kanizsa, *La Grammaire du Voir. Essais sur la perception*, Diderot Editeur, Arts et Sciences, 1997.

[13] M. Kass, A. Witkin, and D. Terzopoulos, *Snakes: Active contour models*, International Journal of Computer Vision, No. 1, 1988, pp. 321-331.

[14] M.-S. Lee and G. Medioni, *Inferred Descriptions in Terms of Curves, Regions and Junctions from Sparse, Noisy Binary Data*, Proceedings of the IEEE International Symposium on Computer Vision, Coral Gable, Florida (Nov. 1995), pp. 73-78.

[15] C. Lopez and J.M. Morel, *Axiomatization of shape analysis and application to texture hyperdiscrimination*, Proceedings of the Trento Conference on Surface Tension and Movement by Mean Curvature, De Gruyter, Berlin, 1992.

[16] R. Malladi, J.A. Sethian, B.C. Vemuri, *A Topology Independent Shape Modeling Scheme*, Proc. SPIE Conf. on Ge-

ometric Methods in Computer Vision II, Vol. 2031, pp. 246-258, San Diego, July 1993.

[17] R. Malladi, J.A. Sethian, B.C. Vemuri, *Evolutionary Fronts for Topology-Independent Shape Modeling and Recovery*, Proceedings of the Third European Conference on Computer Vision, LNCS Vol. 800, pp. 3-13, Stockholm, Sweden, May 1994.

[18] R. Malladi, J.A. Sethian, B.C. Vemuri, *Shape Modeling with Front Propagation: A Level Set Approach*, IEEE Transactions on Pattern Analysis and Machine Intelligence, Vol. 17, No. 2, pp. 158-175, 1995.

[19] D. Mumford and J. Shah, *Optimal approximation by piecewise smooth functions and associated variational problems*, Comm. Pure Appl. Math. 42, 1989, pp. 577-685.

[20] S. Osher and J. A. Sethian, *Fronts Propagating with Curvature-Dependent Speed: Algorithms Based on Hamilton-Jacobi Formulation*, Journal of Computational Physics, 79, pp. 12-49, 1988.

[21] N. Paragios and R. Deriche, *Geodesic Active Regions for Texture Segmentation*, INRIA RR-3440, June 1998.

[22] N. Paragios and R. Deriche, *Geodesic Active Regions for Motion Estimation and Tracking*, INRIA RR-3631, March 1999.

[23] E. Rouy and A. Tourin, *A Viscosity Solutions Approach to Shape-From-Shading*, SIAM J. Numer. Anal., Vol. 29, No. 3, pp. 867-884.

[24] L. Rudin, S. Osher and E. Fatemi, *Nonlinear total variation based noise removal algorithms*, Phys. D 60(1992), pp. 259-268.

[25] K. Siddiqi, Y. B. Lauzière, A. Tannenbaum, and S. W. Zucker, *Area and Length Minimizing Flows for Shape Segmentation*, IEEE Transcations on Image Processing, Vol. 7, No. 3, 1998, pp. 433-443.

[26] M. Sussman, P. Smereka and S. Osher, *A Level Set Approach for Computing Solutions to Incompressible Two-Phase Flow*, J. Comput. Phys., V. 119 (1994), pp. 146-159.

[27] C. Xu, and J. L. Prince, *Snakes, Shapes and Gradient Vector Flow*, IEEE Transcations on Image Processing, Vol. 7, No. 3, 1998, pp. 359-369.

[28] H.-K. Zhao, T. Chan, B. Merriman and S. Osher, *A Variational Level Set Approach to Multiphase Motion*, J. Comput. Phys. 127, 1996, pp. 179-195.

[29] H.-K. Zhao, S. Osher, B. Merriman, and M. Kang, *Implicit, Nonparametric Shape Reconstruction from Unorganized Points Using A Variational Level Set Method*, UCLA CAM Report 98-7 (1998, revised February 1999).